



Transcriptomic and connectomic correlates of differential spatial patterning among gliomas

Rafael Romero-Garcia,^{1,2} Ayan S. Mandal,^{2,3} Richard A. I. Bethlehem,² Benedicto Crespo-Facorro,⁴ Michael G. Hart⁵ and John Suckling^{2,6,7}

Unravelling the complex events driving grade-specific spatial distribution of brain tumour occurrence requires rich datasets from both healthy individuals and patients. Here, we combined open-access data from The Cancer Genome Atlas, the UK Biobank and the Allen Brain Human Atlas to disentangle how the different spatial occurrences of glioblastoma multiforme and low-grade gliomas are linked to brain network features and the normative transcriptional profiles of brain regions.

From MRI of brain tumour patients, we first constructed a grade-related frequency map of the regional occurrence of low-grade gliomas and the more aggressive glioblastoma multiforme. Using associated mRNA transcription data, we derived a set of differential gene expressions from glioblastoma multiforme and low-grade gliomas tissues of the same patients. By combining the resulting values with normative gene expressions from post-mortem brain tissue, we constructed a grade-related expression map indicating which brain regions express genes dysregulated in aggressive gliomas. Additionally, we derived an expression map of genes previously associated with tumour subtypes in a genome-wide association study (tumour-related genes).

There were significant associations between grade-related frequency, grade-related expression and tumour-related expression maps, as well as functional brain network features (specifically, nodal strength and participation coefficient) that are implicated in neurological and psychiatric disorders.

These findings identify brain network dynamics and transcriptomic signatures as key factors in regional vulnerability for glioblastoma multiforme and low-grade glioma occurrence, placing primary brain tumours within a well-established framework of neurological and psychiatric cortical alterations.

- 1 Department of Medical Physiology and Biophysics, Instituto de Biomedicina de Sevilla (IBiS) HUVR/CSIC/Universidad de Sevilla/CIBERSAM, ISCIII, Sevilla, Spain
- 2 Department of Psychiatry, University of Cambridge, Cambridge, UK
- 3 Perelman School of Medicine, University of Pennsylvania, Philadelphia, PA, USA
- 4 Department of Psychiatry, Universidad de Sevilla, Hospital Universitario Virgen del Rocío/IBiS-CSIC/CIBERSAM, ISCIII, Sevilla, Spain
- 5 St George's, University of London & St George's University Hospitals NHS Foundation Trust, Institute of Molecular and Clinical Sciences Neurosciences Research Centre, London, UK
- 6 Behavioural and Clinical Neuroscience Institute, University of Cambridge, Cambridge, UK
- 7 Cambridge and Peterborough NHS Foundation Trust, Cambridge, UK

Received June 20, 2022. Revised August 30, 2022. Accepted September 13, 2022. Advance access publication October 18, 2022

© The Author(s) 2022. Published by Oxford University Press on behalf of the Guarantors of Brain.

This is an Open Access article distributed under the terms of the Creative Commons Attribution-NonCommercial License (<https://creativecommons.org/licenses/by-nc/4.0/>), which permits non-commercial re-use, distribution, and reproduction in any medium, provided the original work is properly cited. For commercial re-use, please contact journals.permissions@oup.com

Correspondence to: Rafael Romero-Garcia
Avenida Doctor Fedriani, S/N
41009, Seville Spain
E-mail: rr480@cam.ac.uk

Keywords: glioma; gene expression; transcriptomic; connectomic

Introduction

Adult diffuse gliomas are devastating and lethal types of cancer. According to the World Health Organization (WHO) grading system, survival rates drastically vary from low-grade gliomas (LGG) with median survival between 4.7 and 9.8 years¹ to glioblastoma multiforme (GBM), or grade IV astrocytoma, with survival limited to ~15 months.² Brain tumours occur via several aetiologies and are located heterogeneously across the brain. Although the location of the tumour determines the likelihood of complete resection, and thus long-term survival,³ its specific location can influence the accompanying cognitive changes that patients often experience. In this study, we leverage well-established open-access data sources to construct a map of the distribution of brain tumours of varying grade, and investigate the reasons for these distributions in the underlying genetic expression and functional networks.

LGGs, most frequently astrocytomas and oligodendrogliomas, are slow-growing, infiltrative tumours that account for 10–20% of all primary brain tumours.¹ Most, usually younger patients, will die due to the malignant (anaplastic) transformation of the tumour to a higher grade. The rate of malignant transformation is diverse amongst patients, and usually determined radiologically. GBM is the most common type of primary malignant brain tumour. In ~90% of cases, they develop *de novo* as primary tumours with a high grade without histological evidence of a precursor lesion.⁴

The traditional grading system based on histological appearance does not always reflect the biological behaviour of tumours, and in 2016 WHO incorporated molecular classification criteria for adult diffuse gliomas that were revisited in 2021 to focus almost exclusively on this approach.^{5,6} A major motivator for this change is that tumour molecular profiles have a greater prognostic value and are better predictors of tumour growth kinetics regardless of grade or histology.^{7,8} For example, mutations of telomerase reverse transcriptase (TERT) and isocitrate dehydrogenase 1 (IDH1-M), methylation of the O-6-methylguanine-DNA methyltransferase gene (MGMT-met) and codeletion of chromosomes 1p and 19q (1p19q-cod) lead to germline variants that are driven by distinct pathogenic mechanisms characterized by specific proliferation rates and aggressiveness. Molecular signature also influences tumour location, with IDH-M gliomas preferentially located in the frontal lobe adjacent to the rostral extension of the lateral ventricles.⁹ It has been hypothesized that the high glutamate flux present in prefrontal cortex creates a metabolic niche that supports IDH-M gliomas.¹⁰ Beyond these well-known genetic mutations, a genome-wide association study (GWAS) including >12 000 glioma patients and 18 000 controls identified 25 risk loci associated with glioma risks in adults.¹¹ These tumour-related genes are heterogeneously distributed across glioma subtypes and grades, suggesting that they also play a major role in tumour appearance and progression.¹²

At the end of the 19th century, Paget described the seed and soil hypothesis that successful tumour growth depends on interactions between the properties of cancer cells (seeds) and their

potential target tissue (soil).^{13,14} Although this hypothesis has been extensively explored as a conceptual scaffold for understanding tumour metastasis, we propose its re-examination in the context of the cellular origins of primary gliomas and their progression.

It has been hypothesized that gliomas originate from neurogenic niches of neuronal-stem cells and oligodendrocyte precursor cells in the subventricular zone¹⁵ that migrate along large-scale axonal tracts to populate distributed cortical areas.¹⁶ Neural-glioma cellular interactions are key determinants of glioma growth and migration¹⁷ forming a positive feedback loop by which glioma progression is promoted by molecules secreted in neuronal communication,¹⁸ and increased glutamate release from gliomas inducing hyperexcitability of cortical networks.¹⁹ We recently demonstrated that regions with a high number of functional connections (i.e. hubs) and with elevated participation coefficient (i.e. regions interconnecting constituent network communities) are more vulnerable to the instantiation of gliomas.²⁰ Collectively, this evidence suggests that structural and metabolic factors are key determinants in tumour progression. However, it neglects the potential contribution of molecular and transcriptomic factors. Here, we investigate whether the cellular and gene expression profiles of the brain regions where glioma cells migrate are related to grade-specific occurrence.

International collaborative efforts have not just generated genomic, epigenomic, transcriptomic, proteomic and neuroimaging data, but have also provided publicly accessible platforms to a growing research community to advance our understanding of the molecular basis of glioma. Datasets incorporating molecular and radiological information are particularly valuable for connecting genotypic and phenotypic profiles. A representative example of this effort is The Cancer Genome Atlas (TCGA)²¹ that, in coordination with The Cancer Imaging Archive (TCIA),²² recruited LGG and GBM patients and gathered transcriptomic data from tumour tissue and MRI scans from the same patients. Despite the unquestionable utility of this resource, gene expression in tumour tissue largely diverges from that in normal tissue, which can be collected from near the tumour but only in a limited number of cases. Complementarily, the Allen Human Brain Atlas (AHBA) currently has the most exhaustive spatial coverage of gene expression data in brain tissue derived from six post-mortem normative donors.²³ Despite these donors having had no brain disease, their spatially resolved gene expression profiles are useful in shedding light on the transcriptomic vulnerabilities of the different brain areas.^{24–26}

In this study, we exploited the TCGA dataset to identify genes differentially expressed in GBM and LGG, and combine these expressions with the AHBA to construct a map of grade-related expression across the entire cortex from normative control data. We additionally incorporated functional connectivity data from the UK Biobank, one of the most ambitious MRI studies to date.²⁷ We hypothesized that LGG and GBM will have a differentiated spatial profiles with higher frontal and parieto-temporal incidence, respectively.^{9,16} Also, that glioma tissue will differentially express

tumour-related genes,¹² and, finally, that those spatial profiles and expression differences are associated in normative post-mortem controls, revealing a grade-sensitive pattern of regional vulnerability to brain tumours.

Materials and methods

TCGA MRI brain tumour masks

The TCGA dataset (<https://www.cancer.gov/about-nci/organization/ccg/research/structural-genomics/tcga/studied-cancers/glioblastoma>) includes solid samples of GBMs and LGGs of which 135 and 107, respectively, were matched to MRI scans from TCIA dataset (<https://wiki.cancerimagingarchive.net/display/Public/Brain-Tumor-Progression>) collected at 13 institutions. Diagnoses of GBM and LGG were established at the contributing institutions and reviewed by neuropathologists in the TCGA consortium (WHO 2016 criteria).^{21,28} Additionally, all transcriptomic and imaging findings described here were reproduced after grouping patients according to the WHO 2021 molecular criteria based on IDH1 mutation status (Supplementary material). This classification included 129 IDH1 wild-type and 88 IDH1 mutated tumours.

T₁-weighted MRIs were skull-stripped, coregistered and re-sampled to 1 mm³ resolution. The segmentation algorithm GLISTRboost was used to classify voxels into four categories: contrast-enhancing tumour, necrotic non-enhancing core, peritumoural oedema and normal brain tissue. Labels were then manually corrected by board-certified neuroradiologists.²⁹ Group-level GBM and LGG occurrence was obtained by concatenating glioma masks across patients. Frequency maps were first calculated at the voxel level as the proportion of times that a given voxel was overlapped by a tumour mask, and then at regional level as the average overlapping of all voxels within each parcel of an atlas. As expression data were primarily available only for one hemisphere, inter-hemispheric differences were not considered here. Accordingly, frequency maps were built by averaging data from left and right hemispheres. See the orange box in Fig. 1 for a summary.

TCGA bulk transcriptomic analysis

Following a previously reported workflow,³⁰ we derived bulk mRNA transcripts of the whole genome (14 899 genes after exclusions) from the $n=672$ individuals from the TCGA dataset. Using the edgeR package,³¹ differential expression analyses compared tissue from patients with GBM ($n=156$) and LGG ($n=516$). As a result, we obtained a log count per million differentiation index per gene where positive values indicate higher expression in GBM compared to LGG bulk tissue. This pipeline was additionally performed by comparing IDH wild-type and IDH mutated bulk tissue to derive differential expression values to establish potential similarities with the grade-related expression. This preprocessing is described in more detail elsewhere.³² Enrichment for cellular and biological components of the resulting differentially expressed genes were assessed using Enrichr (<https://maayanlab.cloud/Enrichr/>).³³

ABHA normative gene expression map

The ABHA provides microarray expression data from six normative donors sampled from >3000 locations that covered the whole left hemisphere and were analysed using >62 000 probes per profile.²³ As the spatial location of the samples was annotated and brains were scanned before tissue resection, it is possible to match a gene expression profile with a specific brain area.³⁴ The dataset

was preprocessed using standard protocols implemented in the Abagen toolbox (<https://abagen.readthedocs.io/>)³⁵: (i) microarray probes were reannotated (probes not matching a valid Entrez ID were discarded); (ii) probes with expression intensity less than the background noise in >50% of samples were discarded; (iii) the probe with the most consistent pattern of regional variation across donors was selected when more than one probe indexed the expression of the same gene; (iv) samples were assigned to a brain region if the coordinates were within 2 mm of the region boundary; and (v) gene expression was normalized across tissue samples.

We used a parcellation resulting from subdividing the Desikan–Killiany anatomical atlas into 316 cortical parcels of approximately equal surface area (~500 mm²; https://github.com/RafaelRomeroGarcia/subParcellation_symmetric).³⁶ All analyses were restricted to the left hemisphere because it was exhaustively covered in all donors. This procedure resulted in a 159 × 15 634 (number of left hemisphere regions × genes) expression matrix describing the complete molecular profile of the normative left hemisphere.

Constructing the grade-related expression map

The differential expression values derived from comparing GBM and LGG bulk tissue from the TCGA dataset were used as weights, where high positive weights correspond with genes that are overexpressed in GBM compared to LGG, and vice versa. These weights were multiplied by the normative expression values across the cortex (ABHA data) to obtain a grade-related expression map. Thus, combining tumour mRNA and the spatial expression of genes in normative individuals, we derived an expression map representing brain regions that tend to express genes that are overexpressed in GBM compared to LGG. This map is hypothesized to reflect transcriptomic vulnerability to GBM. See the purple box in Fig. 1 for a summary.

Principal components of brain-related and tumour-related genes expression

The high coexpression between genes and the spatial distance effect of gene expression (i.e. closer regions tend to have similar expression profiles) implies that the dimensionality of the ABHA data can be effectively reduced to a few components that explain most of the expression variability. We performed a principal component analysis (PCA) over the normative gene expression matrix (159 regions × 15 634 genes) derived from the ABHA to obtain the most relevant regional expression patterns of brain-related genes. As in previous studies, we exploited the first two components (PCA1 and PCA2), resulting in a 159 region × 2 PCA matrix revealing how each of the two gradients weight a given region.³⁷ This linear dimensionality reduction technique allows visual and analytical exploration of the gene expression profiles.

Additionally, we identified a set of 15 genes derived from 25 loci that have been associated with tumour grading in a GWAS study¹²: IDH1, ATRX, TERT, MGMT, EGFR, PDGFRA1, TP53, NF1, MDM2, CDKN2A, CDKN2B, PTEN, PIK3CA, MYCN, CIC, FUBP1, NOTCH1 and PI3K. The same PCA procedure was performed over this set of genes (i.e. using a 159 regions × 15 genes expression matrix) to derive the most relevant regional expression patterns of tumour-related genes. See the green box in Fig. 1 for a summary.

Brain network attributes

The 35 830 individuals that were available and preprocessed by the UK Biobank at the time of these analyses were used to derive

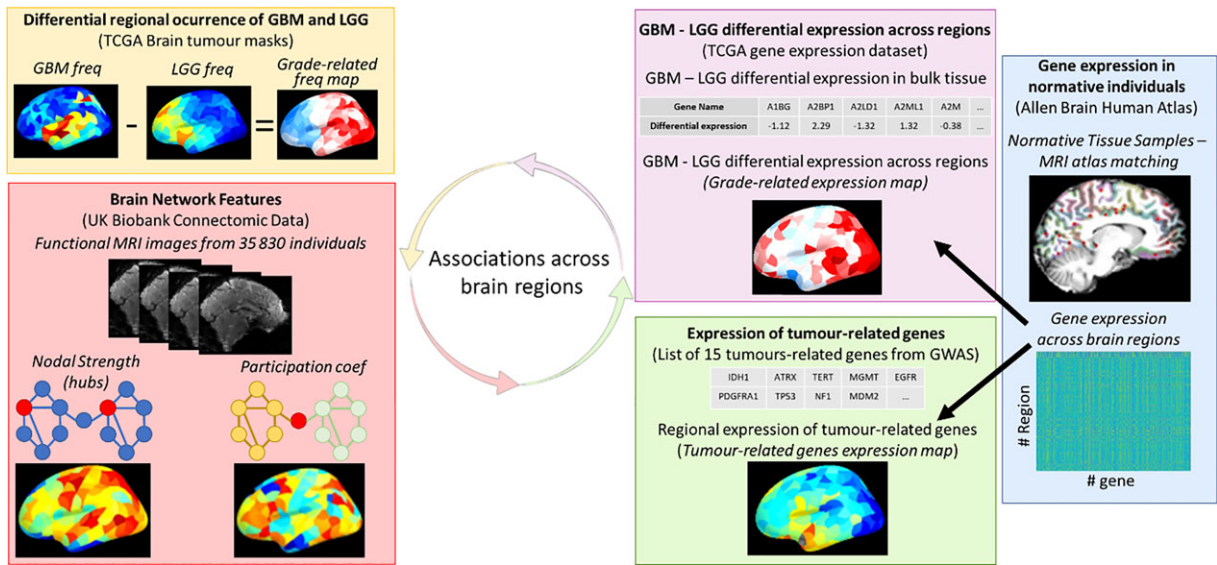


Figure 1 Flow chart of data processing and analysis. Grade-related frequency maps were derived from the TCGA brain tumour masks (top left box) and brain network features were extracted from the UK Biobank fMRI dataset (bottom left box). Grade-related expression regional values (top middle box) were calculated by combining the differential expression in bulk tumour tissue with the ABHA (right box). The spatial expression pattern of 15 genes from a previous GWAS glioma study¹² was computed from the ABHA (bottom middle box).

Table 1 Demographic and clinical variables for 242 patients with glioma from TCIA

Demographic variables	
Age, years	52.9 (15.2)
Gender, male/female/not available	133/107/2
Clinical variables	
Grade, GBM/LGG	135/107
Molecular subtype, IDH-wt/IDH-mut-1p19q-codel/IDH-mut-1p19q-noncode/NA	124/27/61/30

robust brain connectivity markers in normative participants. Preprocessing included motion correction, intensity normalization, high pass temporal filtering, EPI unwarping and artefact removal by ICA + FIX processing, and are described elsewhere.³⁸ Parcellations were transformed from structural T₁-weighted image space to functional (EPI) MRI space using linear transformations. Regional time series were computed as the average time series of all voxels in the grey matter of each region. Functional connectivity between regions was calculated as the Pearson correlation between regional time series.

Nodal strength was calculated for each individual as the average functional connectivity, representing regions that are more strongly functionally synchronized with other regions (hubs). As nodal strength does not account for the community structure of the brain and is influenced by community size,³⁹ we additionally computed participation coefficients (PC) as

$$PC(i) = 1 - \frac{\sum_{s=1}^K k_{i,s}}{k_i}, \tag{1}$$

where K is the number of communities, k_i is the degree of the node i and k_{i,s} is the intra-community degree of node i (representing the inter-modular connections of each node). The participation coefficient captures the nodes that facilitate communication between

communities that make up the brain network. Communities were identified using a consensus approach based on the Louvain algorithm. Because the algorithm is not deterministic, we used consensus clustering to detect a stable community structure (1000 permutations).³⁴ Finally, canonical (group-level) nodal strength and participation coefficient indices used in further analyses were calculated as the average regional values across all individuals. See the red box in Fig. 1 for a summary.

Statistical analyses

Associations were calculated using Pearson correlation when the Kolmogorov-Smirnov tests retained the hypothesis that both the independent and dependent variable arises from standard normal distributions. Spearman's rho correlation was used otherwise.

Both traditional parametric and non-parametric methods for relating brain maps ignore the inherent spatial auto-correlation of brain features (i.e. the data independence assumption is violated). To avoid inflated estimations of significance values, correspondence among regional maps (i.e. gene expression, glioma frequency and network metrics) was statistically tested by generating 10 000 random rotations (i.e. spins) of the cortical parcellation to estimate the distribution of r-values (or rho values for Spearman's correlations) under the null hypothesis. This process provided a reference (null-)distribution for significance testing (P_{spin}) of brain feature associations across regions while controlling for spatial contiguity of the cortical surface.^{40,41} Given that brain lobes have characteristic gene expression patterns, points on scatterplots (representing brain regions) were colour coded according to lobes: frontal (green), parietal (purple), temporal (yellow), occipital (light blue), cingulate (brown) and insula (blue).

Two separate hypotheses were tested when exploring the associations between regional patterns of brain- and tumour-related gene expressions with functional brain network measures and grade-related expression maps: (i) that the associations between both brain-related and tumour-related gene expressions maps with network and grade-related markers across brain regions

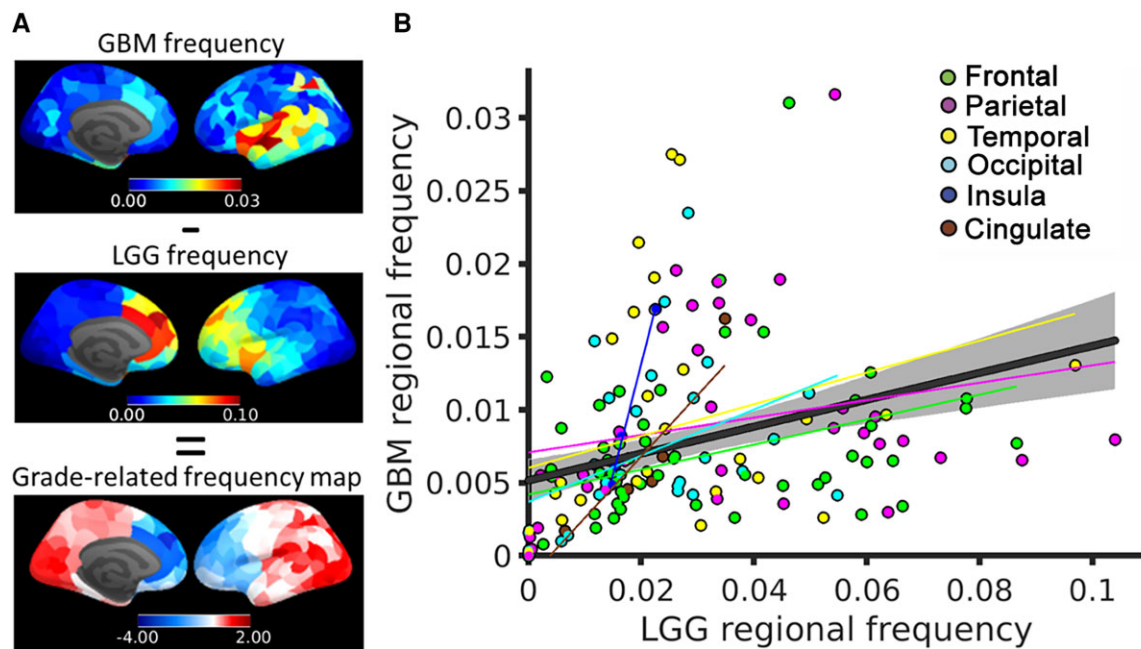


Figure 2 GBM and LGG regional distributions. (A) Grade-related frequency map created from subtracting and z-scoring the GBM and LGG frequencies (i.e. occurrences) across brain regions. (B) Association between LGG and GBM frequencies.

would be significantly different from zero (P_{spin} , computed as described above); and (ii) that the associations between tumour-related gene expression and each marker would be stronger (i.e. explained more variance) than between brain-related genes and each marker (P_{perm}). As tumour-related genes were constituted by 15 genes with an associated coexpression value, each of the 10 000 permutations was calculated by randomly selecting 15 genes with similar coexpression (between 95 and 105% of the real coexpression value) and by correlating them with the regional marker. P_{perm} was then calculated as the proportion of randomly permuted cases that explained more variance than the observed set of tumour-related genes. $P_{\text{perm}} < 0.05$ was the threshold for significance.

Data availability

All data used are publicly available. Anonymized lesion data for GBM and LGG, respectively, are available at: <https://www.cancerimagingarchive.net/access-data/>. Clinical and genomic data from TCGA can be downloaded in R by following the workflow described in <https://www.bioconductor.org/packages/release/workflows/vignettes/TCGAWorkflow/inst/doc/TCGAWorkflow.html>. UK Biobank neuroimaging data are available at: <https://www.fmr.ox.ac.uk/ukbiobank/>.

Results

Regional distributions of GBM and LGG are overlapping, but distinct

Demographic and clinical information regarding the 242 patients with glioma with matched MRI scans from TCIA is included in Table 1. Group-level GBM and LGG occurrence was obtained by concatenating glioma masks across patients (Fig. 1, orange box).

GBM and LGG occurrences were heterogeneously distributed across the cortex with GBM predominantly located in insular and temporal cortices and LGG preferentially presenting in frontal and

insular cortices (Fig. 2A). Consequently, despite the spatial distribution of high and low-grade tumours being significantly correlated ($\rho = 0.54$, $P_{\text{spin}} < 10^{-4}$), a substantial part of the variance remains unexplained (Fig. 2B). Maps were subtracted to construct the grade-related frequency map, a regional map reflecting the preferential occurrence of GBM compared with LGG. This map revealed a gradient of tumour grade occurrence across the cortex, with frontal and insular cortices having greater LGG occurrence and temporal and occipital cortices having greater GBM occurrence.

Genes differentially expressed in GBM and LGG tissues show a characteristic expression pattern across brain regions

We initially determined how each gene of the genome was differentially expressed in GBM compared with LGG bulk tissue using the TCGA dataset (Fig. 1, purple box; Supplementary material). The top 1000 genes showing the highest differentiation between these two grades of glioma were significantly ($P < 10^{-8}$) enriched for neuronal elements, neurotransmitter activity and synaptic transmission by reference to the gene ontology (GO) resource (<http://geneontology.org>) (Table 2 and Supplementary material). Expression values were also computed comparing IDH1 wild-type and IDH1 mutated tumours resulting in a similar differential expression profile (Spearman's $\rho = 0.87$, $P \approx 0$). Correlation between differential expression values was weaker, but still significant when comparing grade-related expression with IDH1 mutated and 1p19q codeleted tumours (Spearman's $\rho = 0.73$, $P \approx 0$), and also with IDH1 mutated and 1p19q non-codeleted tumours (Spearman's $\rho = 0.60$, $P \approx 0$) (Supplementary Fig. 1).

The tumour grade-related expression values were multiplied by the canonical gene expression values from the brain tissue of post-mortem control donors in the AHBA to derive a weighted average of genes differentially expressed in GBM and LGG across regions (Fig. 3A). The resulting grade-related expression map showed that genes overexpressed in GBM tissue are preferentially expressed in

Table 2 Enrichment for molecular function and cellular components of the top 1000 genes with greatest differential expression in GBM and LGG glioma tissues

	P-value	Adjusted P-value	Odds ratio
Molecular function			
Voltage-gated cation channel activity (GO:0022843)	3.03×10^{-10}	1.88×10^{-7}	6.02
Voltage-gated potassium channel activity (GO:0005249)	1.59×10^{-8}	0.0000493	5.82
Ligand-gated cation channel activity (GO:0099094)	3.43×10^{-7}	0.00007108	5.2
GABA receptor activity (GO:0016917)	5.19×10^{-7}	0.00008064	13.26
Calcium-dependent phospholipid binding (GO:0005544)	7.13×10^{-7}	0.00008855	6.75
GABA-gated chloride ion channel activity (GO:0022851)	1.007×10^{-6}	0.00009956	22.32
Transmitter-gated ion channel activity involved in regulation of postsynaptic membrane potential (GO:1904315)	1.122×10^{-6}	0.00009956	9.59
GABA-A receptor activity (GO:0004890)	1.753×10^{-6}	0.000136	13.92
Platelet-derived growth factor binding (GO:0048407)	5.726×10^{-6}	0.0003556	22.93
Calcium ion binding (GO:0005509)	5.467×10^{-6}	0.0003556	2.38
Potassium channel activity (GO:0005267)	1.029×10^{-5}	0.0005808	4.1
Ligand-gated anion channel activity (GO:0099095)	1.497×10^{-5}	0.0007749	12.17
delayed rectifier potassium channel activity (GO:0005251)	2.448×10^{-5}	0.001169	7.18
cation channel activity (GO:0005261)	2.697×10^{-5}	0.001196	3.75
adenylate cyclase inhibiting G protein-coupled glutamate receptor activity (GO:0001640)	3.293×10^{-5}	0.001278	23.86
Cellular components			
Neuron projection (GO:0043005)	3.27×10^{-17}	8.87×10^{-15}	3.33
Collagen-containing extracellular matrix (GO:0062023)	2.65×10^{-14}	3.59×10^{-12}	3.57
Integral component of plasma membrane (GO:0005887)	2.38×10^{-13}	2.15×10^{-11}	2.13
Exocytic vesicle membrane (GO:0099501)	4.70×10^{-7}	0.00002121	7.95
Synaptic vesicle membrane (GO:0030672)	4.70×10^{-7}	0.00002121	7.95
Potassium channel complex (GO:0034705)	3.43×10^{-7}	0.00002121	5.2
GABA-A receptor complex (GO:1902711)	1.753×10^{-6}	0.00006785	13.92
Dendrite (GO:0030425)	2.017×10^{-6}	0.00006832	2.7
Voltage-gated potassium channel complex (GO:0008076)	2.616×10^{-6}	0.00007877	4.97
Axon (GO:0030424)	1.133×10^{-5}	0.0003072	2.82
Postsynaptic density membrane (GO:0098839)	0.0000334	0.0008228	10.3
Postsynaptic specialization membrane (GO:0099634)	4.794×10^{-5}	0.001083	9.56
Dense core granule (GO:0031045)	7.994×10^{-5}	0.001667	11.46
Excitatory synapse (GO:0060076)	0.0001663	0.003218	7.43
Cytoskeleton of presynaptic active zone (GO:0048788)	0.0001926	0.003479	25.43

occipital and parietal cortices, while genes overexpressed in LGG tissue are expressed in anterior cingulate, motor, parahippocampal and entorhinal regions. This pattern was aligned with the two most important gradients of regional expression of 14 899 brain-related genes in healthy individuals as captured by PCA 1 (32% explained variance; $\rho = -0.40$; $P_{\text{spin}} = 0.006$) and PCA 2 (25% explained variance; $\rho = 0.54$; $P_{\text{spin}} = 0.006$) (Fig. 3B, left and C).

Most genes that, according to a previous GWAS study,¹² present frequent molecular alterations on the five WHO 2016 subtypes of adult diffuse glioma (i.e. tumour-related genes) were significantly differentially expressed in GBM and LGG tissues (Fig. 1, green box: 13 of 15 were significant $P_{\text{FDR}} < 0.01$; Supplementary Table 1). When deriving the gene expression profiles of these tumour-related genes from the ABHA dataset (Fig. 1, blue box), we found two principal gradients of expression in healthy individuals: PCA 1 explaining 39% of the variance, PCA 2 explaining 16% of the variance (Fig. 3B, right). Brain-related and tumour-related gene expression were highly correlated across regions (Brain PCA1 versus Tumour PCA1, $\rho = 0.42$, $P_{\text{spin}} = 0.24$; Brain PCA1 versus Tumour PCA2, $\rho = 0.45$, $P_{\text{spin}} = 0.01$; Brain PCA2 versus Tumour PCA1, $\rho = 0.59$, $P_{\text{spin}} = 10^{-4}$; Brain PCA2 versus Tumour PCA2, $\rho = 0.86$, $P_{\text{spin}} < 10^{-4}$; Supplementary Fig. 2).

Tumour-related principal components were also aligned with the grade-related expression map (PCA 1: $\rho = 0.40$; $P_{\text{spin}} = 0.01$;

PCA 2: $\rho = -0.65$; $P_{\text{spin}} = 0.0001$; Fig. 3D). The tumour-related genes expression map significantly explained more variance of the grade-related gene expression map than randomly selected sets of brain-related genes under a null hypothesis (10 000 permutations preserving the number of tumour-related genes and their coexpression, $P_{\text{perm}} = 0.003$). Despite both expression maps being constructed using different approaches (i.e. considering genes differentially expressed in tumour tissue and GWAS-derived genes¹²), they both captured a similar transcriptional gradient of tumour grade vulnerability. Differential expression values derived from comparing IDH1 wild-type versus IDH mutated tumour tissue were more strongly associated with tumour-related genes than with brain-related genes ($P_{\text{perm}} = 0.008$; Supplementary Fig. 3).

Tumour grade-related frequency is associated with brain network features

We compared the glioma frequency maps with regional brain network measurements derived from healthy individuals of the UK BioBank dataset: nodal strength (i.e. regions that are more strongly functionally synchronized) and participation coefficient (i.e. regions with more inter-modular connections) (Fig. 1, red box). As expected, modular partition resembled known subnetworks of the brain (Supplementary Fig. 4). The GBM frequency map was

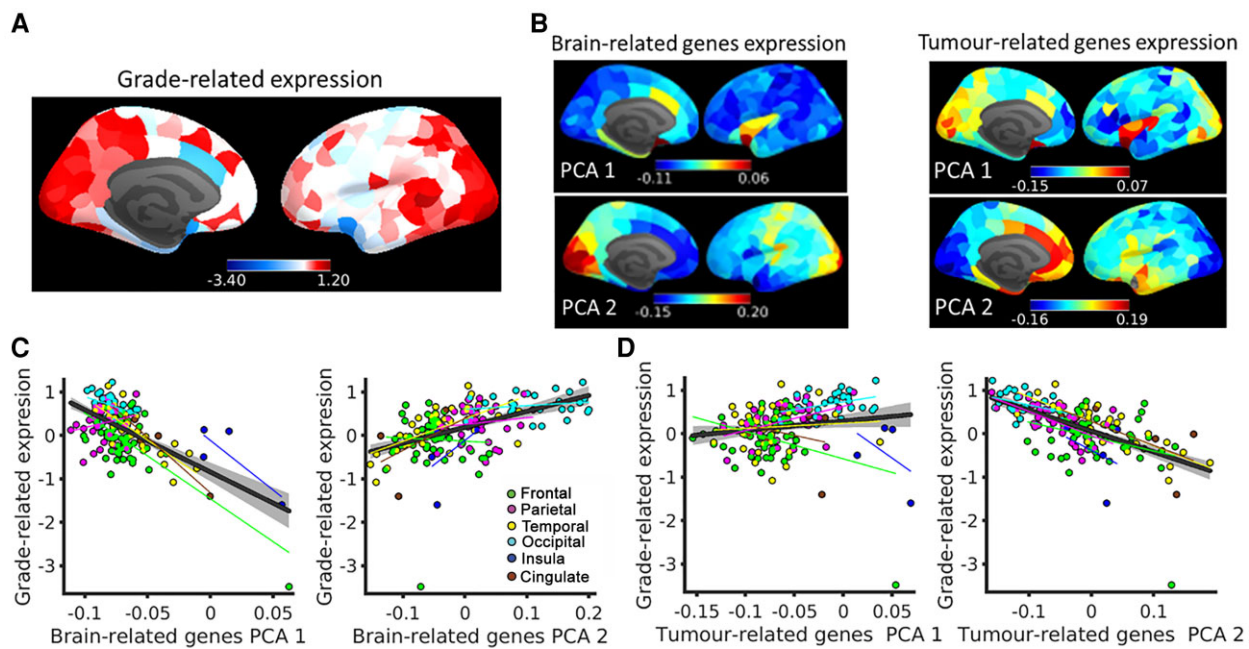


Figure 3 Regional pattern of genes differentially expressed in GBM and LGG tissues and tumour-related genes. (A) Regional expression of brain-related genes in controls weighted by differential expression in GBM and LGG tissues (z-scored). (B) Regional expression pattern derived from the ABHA of the first and second principal components of brain-related (left) and tumour-related (right) genes. (C) Association between grade-related expression (shown in A) and the first and second principal components of brain-related genes from the ABHA. (D) Association between grade-related expression and principal components of tumour-related gene expression.

correlated with participation coefficient ($\rho = 0.24$; $P_i = 0.0026$), but not nodal strength ($\rho = 0.14$; $P_{\text{spin}} = 0.09$; Fig. 4A). Conversely, the LGG frequency map was significantly correlated with nodal strength ($\rho = -0.42$; $P_{\text{spin}} = 0.0001$), but not participation coefficient ($\rho = 0.03$; $P_{\text{spin}} = 0.71$; Fig. 4B). Similar results were obtained when considering the IDH1 wild-type versus mutated classification (Supplementary Fig. 5).

This evidence indicates that regions playing a central role in healthy brain network topology may be key sites of vulnerability for aggressive tumours.

The regional expression pattern of genes differentially expressed in GBM and LGG tissues is associated with grade-related frequency and brain network features

We next compared the regional patterns of the grade-related gene expression (Fig. 3) with brain network features (Fig. 4). Grade-related gene expression was not associated with glioma frequency (GBM and LGG occurrences combined; $R^2 = 0.15$; $P_{\text{spin}} = 0.127$), but was significantly associated with the grade-related frequency map (difference between GBM and LGG occurrences; $\rho = 0.51$; $P_{\text{spin}} = 0.038$; Fig. 5A). In other words, the grade-related gene expression pattern is related to the gradient of tumour grade occurrence across the cortex rather than with the total (pooled) tumour occurrence.

When comparing the grade-related gene expression with brain network features we found that it was significantly associated with both nodal strength ($R^2 = 0.11$; $P_{\text{spin}} = 0.006$) and participation coefficient ($R^2 = 0.07$; $P_{\text{spin}} = 0.016$; Fig. 5B). Similar results were found when comparing IDH1-related gene expression with glioma frequency ($R^2 = 0.20$; $P_{\text{spin}} = 0.15$), IDH1-related frequency ($\rho = 0.51$; $P_{\text{spin}} = 0.04$) and brain network features (nodal strength, $\rho = 0.33$; $P_{\text{spin}} = 0.01$; participation coefficient, $\rho = 0.24$; $P_{\text{spin}} = 0.036$)

(Supplementary Fig. 6). These associations suggest that specific network features and normative gene expression contribute to regional vulnerability for aggressive tumours.

Expression of tumour-related genes is associated with grade-related frequency map and with nodal strength

The regional expression pattern of tumour-related genes was associated with grade-related frequency and brain network features. Specifically, grade-related frequency was significantly associated with tumour-related PCA 2 ($\rho = -0.64$; $P_{\text{spin}} = 0.003$), but not PCA 1 ($\rho = 0.42$; $P_{\text{spin}} = 0.08$) (Fig. 6A). Similarly, PCA 2 but not PCA 1 was associated with both brain network features: nodal strength (Fig. 6B) and participation coefficient (Fig. 6C) (nodal strength: PCA 1, $\rho = 0.32$; $P_{\text{spin}} = 0.08$; nodal strength: PCA 2, $\rho = -0.51$; $P_{\text{spin}} = 0.003$; participation coefficient: PCA 1, $\rho = 0.17$; $P_{\text{spin}} = 0.12$; participation coefficient: PCA 2, $\rho = -0.26$; $P_{\text{spin}} = 0.039$).

Associations were stronger for PCA 2 of tumour-related genes than for PCA 2 of brain-related genes (10 000 permutations; grade-related frequency $P_{\text{perm}} = 0.006$; nodal strength $P_{\text{perm}} = 0.004$; participation coefficient; $P_{\text{perm}} = 0.004$). This ordering of effect sizes in the relationships between tumour-related gene expression and network features, and grade-related frequency recapitulate our findings using the gene set derived by GWAS (Fig. 3).

Discussion

Glioma occurrence across the cortex is not random, but is greater in frontal, temporal and insular lobes.^{42,43} From previous work that identified both genetics and brain function as key factors determining the spatial distribution of glioma,²⁰ we hypothesized that they

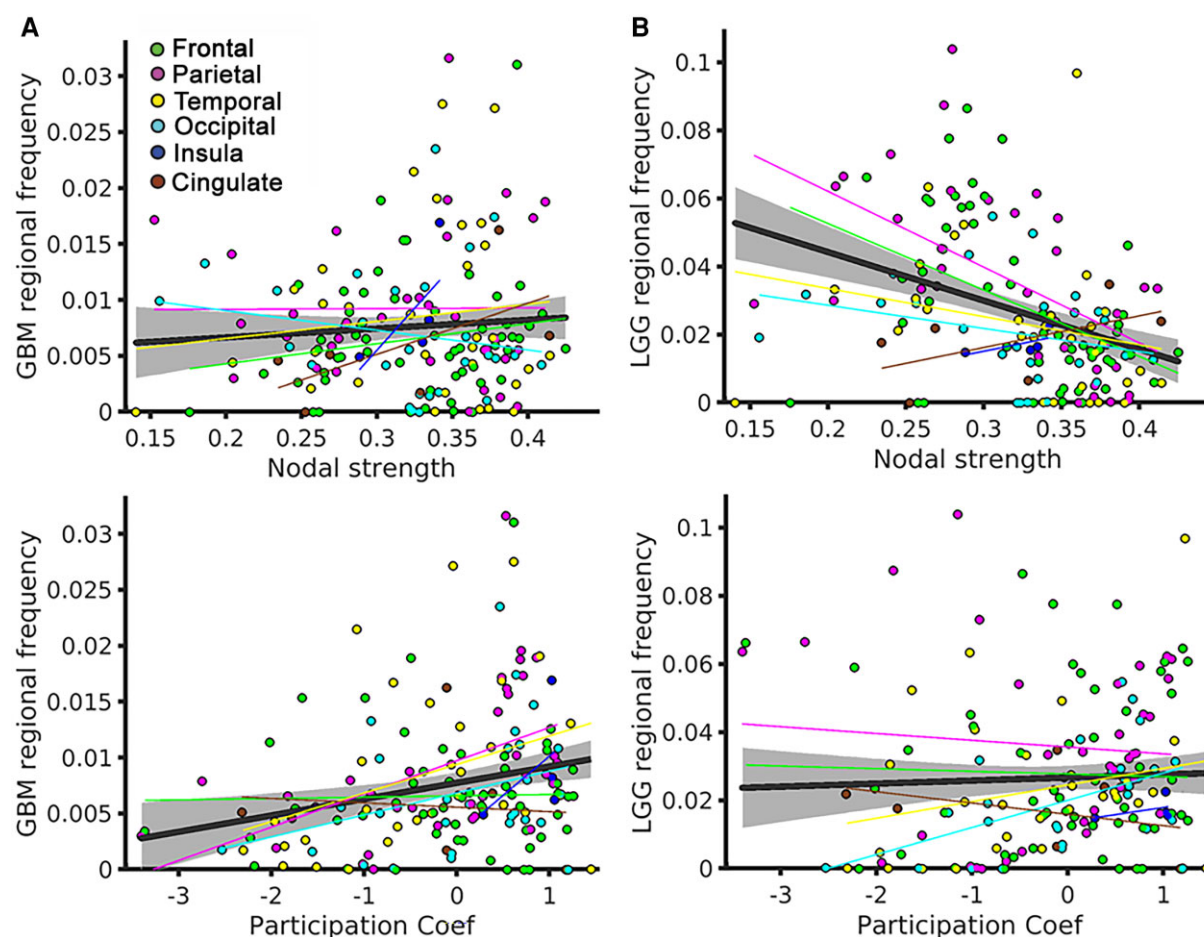


Figure 4 The regional distribution of GBMs and LGGs is associated with brain network features. (A) Association between GBM regional frequency and nodal strength and participation coefficient. (B) Association between LGG regional frequency and nodal strength and participation coefficient.

would similarly influence the differential pattern of occurrence related to tumour grade. Indeed, the transcriptomic and connectomic vulnerability factors in tumour emergence remain incompletely explored.⁴⁴

We have shown that the pattern of differentially expressed genes in GBM and LGG tissues matches the corresponding frequency of their differential (i.e. grade-related) occurrence. Furthermore, the pattern of differentially expressed genes is also related to the topology and magnitude of the functional connectivity network, and to the expression of well-established tumour-related genes in normative controls. In combination, we found significant associations between functional connectivity, tumour-related gene expression and grade-related glioma frequency.

The interaction between glioma and neuronal elements has been known for over 80 years since H. J. Scherer noted the predilection for gliomas to grow along and around normal neurons.⁴⁵ Using MRI, we found that the GBM, but not the LGG frequency distribution was significantly associated with the participation coefficient of functional networks in a way that suggests that bridges interconnecting constituent communities are more vulnerable to the appearance of malignant tumours. Interestingly, functional network architecture, particularly regions with high connectivity, has been reproducibly linked with structural changes characteristic of psychiatric and neurological diseases.^{46,47}

An extensive literature demonstrates that gliomas are electrically and synaptically integrated into neural circuits. Micro-scale

experimental studies in animal models indicate that electrochemical communication occurs through bona fide AMPA receptor-dependent neuron-glioma synapses.⁴⁸ At the macroscale circuit level, Numan et al.⁴⁹ describe gliomas with increased malignancy preferentially occurring in regions characterized by higher brain activity in human controls. Functional brain networks have also been implicated as the substrate for structural lesions in a wide variety of psychiatry disorders, and appear to influence the location of primary tumours, albeit with a reduced effect size relative to genetic coexpression.¹⁶ Additionally, tumour functional integration within the global brain signal has been linked with cognitive recovery after glioma surgery.⁵⁰ This study demonstrates that the principle of intimate entanglement between brain networks and patterns of neuropathological change is also relevant to tumour emergence and development.

Understanding the interplay between the molecular alterations that occur in gliomas and the transcriptomic signature of the normative brain identifies vulnerability factors that help explain the origins and progression of tumours. Here, we found that the differential expression profiles between GBM and LGG tissues were associated with the expression of brain-related genes and tumour-related genes (previously identified in the literature) in normative controls. The association with brain-related genes is probably mediated by cell type as the main contributing factor of the regional expression profile.⁵¹ Accordingly, Tan et al.⁵² reported the first PCA component of the ABHA dataset as composed of two

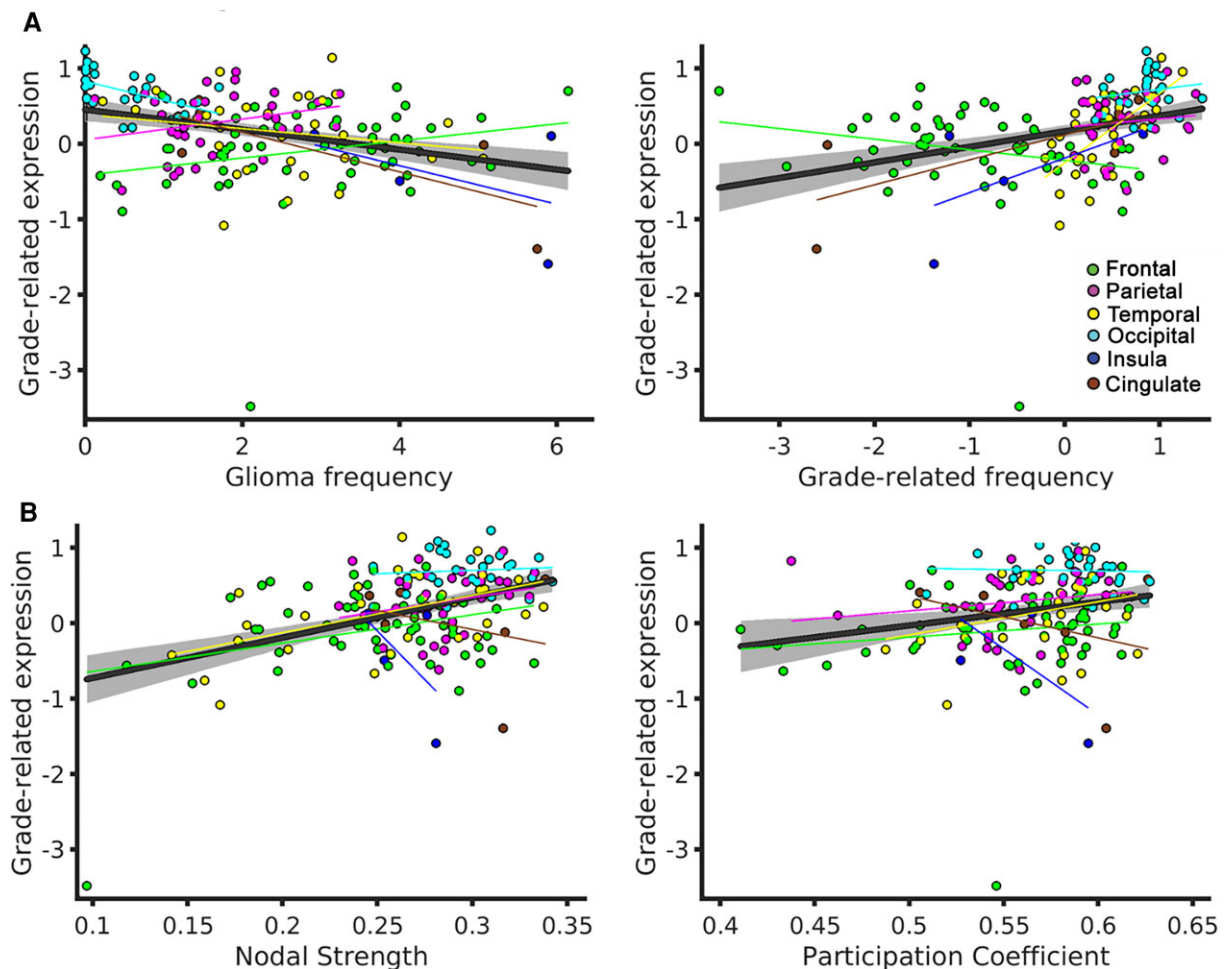


Figure 5 Genes differentially expressed in glioma tissue are associated with imaging markers. (A) Grade-related gene expression association with glioma frequency (i.e. GBM and LGG occurrences combined) and grade-related frequency. (B) Grade-related gene expression association with brain network nodal strength and participation coefficient.

anti-correlated patterns enriched in oligodendrocyte and neuronal markers, respectively: a pattern that has been also described in the mouse brain.⁵³ The potential role of neuronal components in the distribution of gliomas is additionally supported by the enrichment of neuronal elements, neurotransmitter activity and synaptic transmission that were found in the GO analysis of the GBM and LGG tissues. Variance of the grade-related gene expression map was significantly better explained by PCA2 expression patterns for tumour-related than for brain-related genes (despite being partially overlapped), indicating that cell types are only one contributing factor.

Transcriptomic risk factors of glioma occurrence are poorly understood due to limited data on healthy brain tissue. Conversely, the genetic vulnerability of glioma has been widely studied. The contribution of environmental factors is small (except for moderate to high doses of ionizing radiation) compared with genetic risk.⁵⁴ For example, first-degree relatives of glioma patients have a 2-fold increased risk of developing primary brain tumours compared with first-degree relatives of unaffected individuals.^{55,56} Genetic vulnerability does not only influence the risk of glioma appearance, but also the susceptibility to GBM and non-GBM tumours, reflecting their different aetiologies.¹¹ How a molecular signature impacts prognosis is still a matter of debate. It has been proposed that specific molecular profiles allow more time for neuroplastic

reorganization, reducing the 'lesion momentum' and improving not only survival rates, but also having a protective effect on neuro-cognitive functioning.⁵⁷

Using similar approaches that exploit the ABHA dataset, several studies have shown regional expression patterns in normative controls that can be linked to structural and functional brain alterations of disease-related genes in psychiatric^{24–26} and neurological^{58,59} conditions. Here we extended, for the first time, this principle of transcriptomic vulnerability to neuro-oncology by showing that grade-related occurrence was associated with the expression in controls of tumour-related genes and genes that were differentially expressed in GBM and LGG.

Despite the discovery by GWAS of 25 susceptibility variants associated with GBM and non-GBM tumours, the expression profile across the normative cortex of the associated genes remains to be explored. Characterizing the transcriptomic signature is particularly important for understanding causal genetic associations in this context because most of the 25 loci reside in non-coding regions.¹¹ Complementarily, a recent transcriptomic-wide association study identified 31 genes differentially expressed in GBM and non-GBM tumours,⁶⁰ highlighting the important role that expression regulation has on tumour grade. For this reason, here we augmented the analysis of tumour-related genes (identified by the 25 loci) with a gene expression weighted average based on the differential expression between GBM and LGG bulk

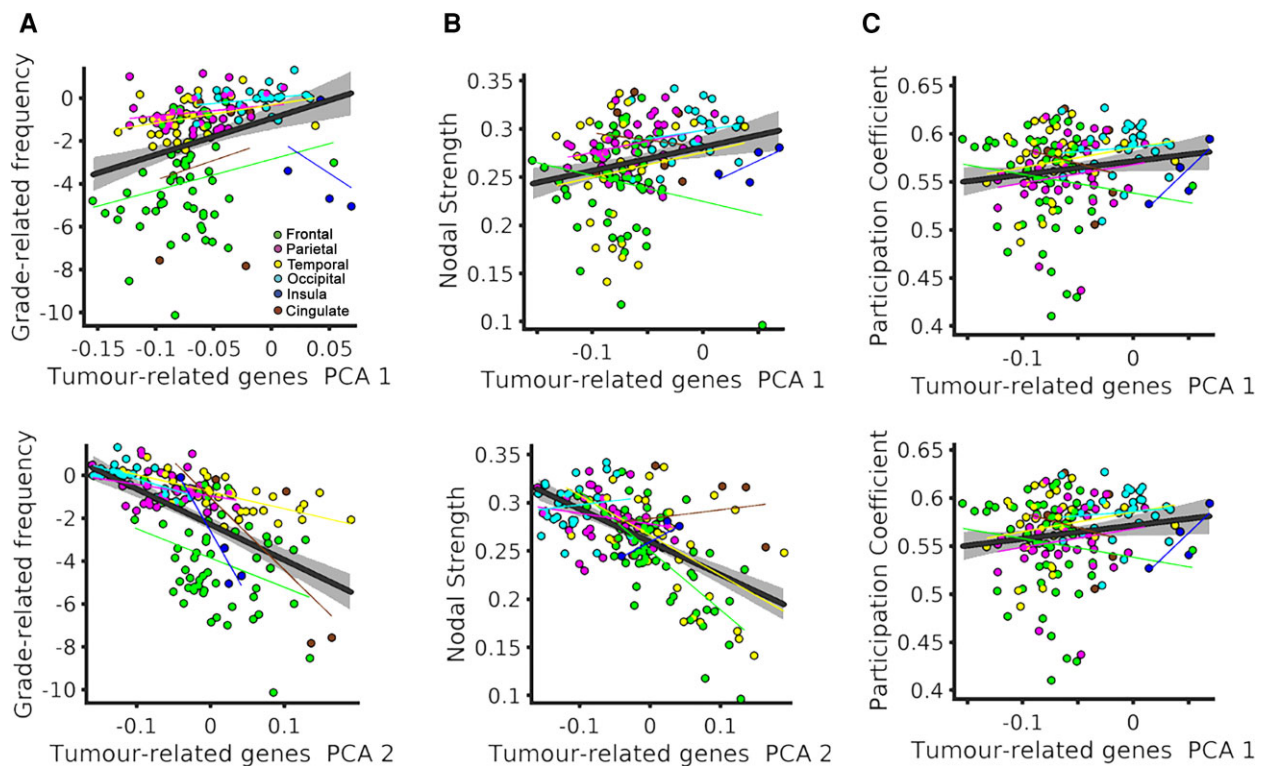


Figure 6 Associations between expression of grade-related frequency, tumour-related genes and brain network markers. (A) Association between the two principal components of tumour-related gene expression and grade-related frequency. (B) Association between the two principal components of tumour-related gene expression and network nodal strength. (C) Association between the two principal components of tumour-related gene expression and network participation coefficient.

tissues. We found not only a significant association between both regional expression patterns, but also with connectivity features.

What emerges from these investigations is that a correspondence between tumour and brain genetic expression is an important factor in the instantiation of tumour cells at particular locations in the cerebral cortex. This goes some way to explaining the heterogeneous distribution of GBM and LGG, which has a clear anterior–posterior gradient in differential frequency of occurrence (Fig. 2). A large component of variance of the grade-related gene expression was significantly related to the grade-related frequency map (Fig. 5), which was supported by the significant association of the regional expression pattern of tumour-related genes with grade-related frequency (Fig. 6). Thus, as an overall motivating framework the seed-and-soil hypothesis, first suggested for brain metastases, could also be invoked for primary tumours, with the genetic signature of precursor cells (seed) and later the tumour itself, preferentially locating in brain regions with an appropriate gene expression (soil).

The success of this framework depends on the accommodation of other well-replicated factors that lie beyond the scope of this article. Age is a key factor, with GBM typically occurring in older adults relative to LGG, and a higher incidence in males relative to females.⁶¹ Although genes are crucial to understanding cancer and its treatment, our comprehension of genetic expression in brain remains incomplete and at an early stage. Nevertheless, it appears that there is variation of gene expression between the sexes⁶² and across the lifespan in a sex-dependent manner.⁶³ As further, more detailed genetic data become available it should be possible to test whether these broad differences are sufficient to explain the observed patterns as part of a seed-and-soil approach.

The reported frequency of LGGs undergoing malignant transformation ranges from 25% to 72%.^{64,65} On the basis of the analyses here,

and if the seed-and-soil hypothesis is adopted, then we can hypothesize that the probability of transformation is dependent on the degree of grade-related gene coexpression between tumour and brain. Circumstantial evidence for this comes from the identification of molecular classification of the tumour as well as male sex as risk factors for transformation.⁶⁴ Our hypothesis would suggest that transforming tumours will be heterogeneously distributed across the brain, although to our knowledge this has not yet been measured.

Overall, given the myriad of studies that have linked brain conditions with normative expression, it is likely that the complex genetic architecture of brain diseases points towards a combined effect of genetic variants and transcriptomic factors that underlie regional brain vulnerability.³⁷

Limitations

As established by the WHO in 2016, the criteria to separate LGG and GBM are largely based on tumour histogenesis, which classifies gliomas according to microscopic features reflecting different putative cells of origin and levels of differentiation.⁵ However, given that tumour molecular features have greater prognostic value than histological markers,^{7,8} the classification protocol was revised in the fifth edition in 2021 advancing the role of molecular diagnosis.⁶ Results presented in this paper are based on the WHO 2016 approach with a reanalysis based on the IDH1 mutation status (WHO 2021) included in the [Supplementary material](#).

An intrinsic limitation of combining datasets from normative individuals (UK Biobank and ABHA) is that templates do not contain information about the brains of glioma patients (TCGA dataset). As a result, neurotypical functional networks and regional gene

expression maps are averages of a normative sample and are not sensitive to intrinsic interindividual differences, omitting important tumour-specific idiosyncrasies.⁴⁴

The brain tissue samples used for RNA sequencing in the AHBA were not homogeneously distributed across the cortex, so estimates of regional expression are based on different numbers of experimental measurements at each of the 159 regions. However, equally sized regions were used to minimize the heterogeneity of sample distribution. Additionally, samples could not be matched across datasets for changes across the life span of gene expression⁶⁶ profiles and functional connectivity.⁶⁷

Conclusions

Regional vulnerability to glioma frequency of occurrence is associated with normative brain expression patterns of tumour-related genes and grade-related differentially expressed genes. Moreover, this tumour grade-related regional vulnerability was associated with features of the functional connectivity network suggesting an interaction between tumour molecular, histological and functional brain architecture. Despite the limitations of establishing associations between multimodal markers derived from individuals with different demographic and clinical profiles, our study demonstrates the potential of combining transcriptomic data with MRI for a richer understanding of the neuropathological processes disrupting brain functioning in patients that can adversely affect quality of life.

Acknowledgements

We thank TCIA and TCGA for access to the neuroimaging and genomic data used in this study, as well as the patients who participated in those projects. This research also relied on imaging data from UK BioBank and The Allen Brain Institute. All research at the Department of Psychiatry in the University of Cambridge is supported by the NIHR Cambridge Biomedical Research Centre (BRC-1215-20014) and NIHR Applied Research Centre. The views expressed are those of the author(s) and not necessarily those of the NIHR or the Department of Health and Social Care.

Funding

R.R.-G. is funded by a non-clinical post-doctoral Brain fellowship, the EMERGIA Junta de Andalucía program (EMERGIA20_00139) and Cancer Research UK Cambridge Centre (grant ref. A25117) and the Plan Propio of the University of Seville.

Competing interests

The authors report no competing interests.

Supplementary material

Supplementary material is available at *Brain* online.

References

- Kumthekar P, Raizer J, Singh S. Low-grade glioma. *Cancer Treat Res*. 2015;163:75–87.
- Chang K, Zhang B, Guo X, et al. Multimodal imaging patterns predict survival in recurrent glioblastoma patients treated with bevacizumab. *Neuro Oncol*. 2016;18:1680–1687.
- Walid MS. Prognostic factors for long-term survival after glioblastoma. *Perm J*. 2008;12:45–48.
- Ohgaki H, Kleihues P. The definition of primary and secondary glioblastoma. *Clin Cancer Res*. 2013;19:764–772.
- Louis DN, Perry A, Reifenberger G, et al. The 2016 World Health Organization classification of tumors of the central nervous system: A summary. *Acta Neuropathol*. 2016;131:803–820.
- Louis DN, Perry A, Wesseling P, et al. The 2021 WHO classification of tumors of the central nervous system: A summary. *Neuro Oncol*. 2021;23:1231–1251.
- Ceccarelli M, Barthel FP, Malta TM, et al. Molecular profiling reveals biologically discrete subsets and pathways of progression in diffuse glioma. *Cell*. 2016;164:550–563.
- Baldock AL, Ahn S, Rockne R, et al. Patient-specific metrics of invasiveness reveal significant prognostic benefit of resection in a predictable subset of gliomas. *PLoS One*. 2014;9:e99057.
- Tejada Neyra MA, Neuberger U, Reinhardt A, et al. Voxel-wise radiogenomic mapping of tumor location with key molecular alterations in patients with glioma. *Neuro Oncol*. 2018;20:1517–1524.
- Chen R, Nishimura MC, Kharbanda S, et al. Hominoid-specific enzyme GLUD2 promotes growth of IDH1R132H glioma. *Proc Natl Acad Sci U S A*. 2014;111:14217–14222.
- Melin BS, Barnholtz-Sloan JS, Wrensch MR, et al. Genome-wide association study of glioma subtypes identifies specific differences in genetic susceptibility to glioblastoma and non-glioblastoma tumors. *Nat Genet*. 2017;49:789–794.
- Molinari AM, Taylor JW, Wiencke JK, Wrensch MR. Genetic and molecular epidemiology of adult diffuse glioma. *Nat Rev Neurol*. 2019;15:405–417.
- Ramakrishna R, Rostomily R. Seed, soil, and beyond: The basic biology of brain metastasis. *Surg Neurol Int*. 2013;4:S256–S264.
- Paget S. The distribution of secondary growths in cancer of the breast. *Lancet*. 1889;133:571–573.
- Sanai N, Alvarez-Buylla A, Berger MS. Neural stem cells and the origin of gliomas. *N Engl J Med*. 2005;353:811–822.
- Mandal AS, Romero-Garcia R, Seidlitz J, Hart MG, Alexander-Bloch AF, Suckling J. Lesion covariance networks reveal proposed origins and pathways of diffuse gliomas. *Brain Commun*. 2021;3:fcab289.
- Gillespie S, Monje M. An active role for neurons in glioma progression: Making sense of Scherer's structures. *Neuro Oncol*. 2018;20:1292–1299.
- Monje M. Synaptic communication in brain cancer. *Cancer Res*. 2020;80:2979–2982.
- Campbell SL, Buckingham SC, Sontheimer H. Human glioma cells induce hyperexcitability in cortical networks. *Epilepsia*. 2012;53:1360–1370.
- Mandal AS, Romero-garcia R, Hart MG, Suckling J. Genetic, cellular, and connectomic characterization of the brain regions commonly plagued by glioma. *Brain*. 2020;143:3294–3307.
- Cancer Genome Atlas Research Network, Brat DJ, Verhaak RGW, et al. Comprehensive, integrative genomic analysis of diffuse lower-grade gliomas. *N Engl J Med*. 2015;372:2481–2498.
- Clark K, Vendt B, Smith K, et al. The Cancer Imaging Archive (TCIA): Maintaining and operating a public information repository. *J Digit Imaging*. 2013;26:1045–1057.
- Hawrylycz MJ, Lein ES, Guillozet-Bongaarts AL, et al. An anatomically comprehensive atlas of the adult human brain transcriptome. *Nature*. 2012;489:391–339.
- Romero-Garcia R, Seidlitz J, Whitaker KJ, et al. Schizotypy-related magnetization of cortex in healthy adolescence is colocated with expression of schizophrenia-related genes. *Biol Psychiatry*. 2020;88:248–259.
- Romero-Garcia R, Hook RW, Tiego J, et al. Brain micro-architecture and disinhibition: A latent phenotyping study across 33 impulsive

- and compulsive behaviours. *Neuropsychopharmacology*. 2021;46:423–431.
26. Romero-Garcia R, Warrier V, Bullmore ET, Baron-Cohen S, Bethlehem RAI. Synaptic and transcriptionally downregulated genes are associated with cortical thickness differences in autism. *Mol Psychiatry*. 2019;24:1053–1064.
 27. Sudlow C, Gallacher J, Allen N, et al. UK Biobank: An open access resource for identifying the causes of a wide range of complex diseases of middle and old age. *PLoS Med*. 2015;12:e1001779.
 28. McLendon R, Friedman A, Bigner D, et al. Comprehensive genomic characterization defines human glioblastoma genes and core pathways. *Nature*. 2008;455:1061–1068.
 29. Schmainda K, Prah M. The Cancer Imaging Archive. Published online 2018.
 30. Silva TC, Colaprico A, Olsen C, et al. TCGA Workflow: Analyze cancer genomics and epigenomics data using Bioconductor packages. *F1000Res*. 2016;5:1542.
 31. Robinson MD, McCarthy DJ, Smyth GK. Edger: A Bioconductor package for differential expression analysis of digital gene expression data. *Bioinformatics*. 2009;26:139–140.
 32. Bakas S, Akbari H, Sotiras A, et al. Advancing The Cancer Genome Atlas glioma MRI collections with expert segmentation labels and radiomic features. *Sci Data*. 2017;4:170117.
 33. Chen EY, Tan CM, Kou Y, et al. Enrichr: Interactive and collaborative HTML5 gene list enrichment analysis tool. *BMC Bioinf*. 2013;14:128.
 34. Romero-Garcia R, Whitaker KJ, Váša F, et al. Structural covariance networks are coupled to expression of genes enriched in supragranular layers of the human cortex. *Neuroimage*. 2018;171:256–267.
 35. Markello RD, Arnatkeviciute A, Poline JB, Fulcher BD, Fornito A, Misic B. Standardizing workflows in imaging transcriptomics with the abagen toolbox. *eLife*. 2021;10:e72129.
 36. Romero-Garcia R, Atienza M, Clemmensen LH, Cantero JL. Effects of network resolution on topological properties of human neocortex. *Neuroimage*. 2012;59:3522–3532.
 37. Keo A, Mahfouz A, Ingrassia AMT, et al. Transcriptomic signatures of brain regional vulnerability to Parkinson's disease. *Commun Biol*. 2020;3:101.
 38. Alfaro-Almagro F, Jenkinson M, Bangerter NK, et al. Image processing and quality control for the first 10,000 brain imaging datasets from UK biobank. *Neuroimage*. 2018;166:400–424.
 39. Power JD, Schlaggar BL, Lessov-Schlaggar CN, Petersen SE. Evidence for hubs in human functional brain networks. *Neuron*. 2013;79:798–813.
 40. Váša F, Seidlitz J, Romero-Garcia R, et al. Adolescent tuning of association cortex in human structural brain networks. *Cereb Cortex*. 2018;28:281–294.
 41. Alexander-Bloch AF, Shou H, Liu S, et al. On testing for spatial correspondence between maps of human brain structure and function. *Neuroimage*. 2018;178:540–551.
 42. Larjavaara S, Mäntylä R, Salminen T, et al. Incidence of gliomas by anatomic location. *Neuro Oncol*. 2007;9:319–325.
 43. Duffau H, Capelle L. Preferential brain locations of low-grade gliomas. *Cancer*. 2004;100:2622–2626.
 44. Germann J, Zadeh G, Mansouri A, Kucharczyk W, Lozano AM, Boutet A. Untapped neuroimaging tools for neuro-oncology: Connectomics and spatial transcriptomics. *Cancers (Basel)*. 2022;14:464.
 45. Scherer HJ. Structural development in gliomas. *Am J Cancer*. 1938;34:333–351.
 46. Seeley WW, Crawford RK, Zhou J, Miller BL, Greicius MD. Neurodegenerative diseases target large-scale human brain networks. *Neuron*. 2009;62:42–52.
 47. Crossley NA, Mechelli A, Scott J, et al. The hubs of the human connectome are generally implicated in the anatomy of brain disorders. *Brain*. 2014;137:2382–2395.
 48. Venkatesh HS, Morishita W, Geraghty AC, et al. Electrical and synaptic integration of glioma into neural circuits. *Nature*. 2019;573:539–545.
 49. Numan T, Breedts LC, Maciel BAPC, et al. Regional healthy brain activity, glioma occurrence and symptomatology. *medRxiv*. Preprint. Published online 1 January 2022.
 50. Romero-Garcia R, Hart MG, Bethlehem RAI, et al. Bold coupling between lesioned and healthy brain is associated with glioma patients' recovery. *Cancers (Basel)*. 2021;13:5008.
 51. Cahoy JD, Emery B, Kaushal A, et al. A transcriptome database for astrocytes, neurons, and oligodendrocytes: A new resource for understanding brain development and function. *J Neurosci*. 2008;28:264–278.
 52. Tan PPC, French L, Pavlidis P. Neuron-enriched gene expression patterns are regionally anti-correlated with oligodendrocyte-enriched patterns in the adult mouse and human brain. *Front Neurosci*. 2013;7:5.
 53. French L, Tan PPC, Pavlidis P. Large-scale analysis of gene expression and connectivity in the rodent brain: Insights through data integration. *Front Neuroinform*. 2011;5:12.
 54. Kinnerley B, Labussière M, Holroyd A, et al. Genome-wide association study identifies multiple susceptibility loci for glioma. *Nat Commun*. 2015;6:8559.
 55. Hemminki K, Tretli S, Sundquist J, Johannesen TB, Granström C. Familial risks in nervous-system tumours: A histology-specific analysis from Sweden and Norway. *Lancet Oncol*. 2009;10:481–488.
 56. Malmer B, Grönberg H, Bergenheim AT, Lenner P, Henriksson R. Familial aggregation of astrocytoma in Northern Sweden: An epidemiological cohort study. *Int J Cancer*. 1999;81:366–370.
 57. Wefel JS, Noll KR, Scheurer ME. Neurocognitive functioning and genetic variation in patients with primary brain tumours. *Lancet Oncol*. 2016;17:e97–e108.
 58. Seidlitz J, Nadig A, Liu S, et al. Transcriptomic and cellular decoding of regional brain vulnerability to neurogenetic disorders. *Nat Commun*. 2020;11:3358.
 59. Kang S, Kim HR, Seong JK. Associating cognitive reserve and brain-wide gene expression regarding Alzheimer's disease. *Alzheimer's Dement*. 2021;17:e049732.
 60. Atkins I, Kinnerley B, Ostrom QT, et al. Transcriptome-wide association study identifies new candidate susceptibility genes for glioma. *Cancer Res*. 2019;79:2065–2071.
 61. Chakrabarti I, Cockburn M, Cozen W, Wang YP, Preston-Martin S. A population-based description of glioblastoma multiforme in Los Angeles County, 1974–1999. *Cancer*. 2005;104:2798–2806.
 62. Gegenhuber B, Tollkuhn J. Signatures of sex: Sex differences in gene expression in the vertebrate brain. *Wiley Interdiscip Rev Dev Biol*. 2020;9:e348.
 63. Berchtold NC, Cribbs DH, Coleman PD, et al. Gene expression changes in the course of normal brain aging are sexually dimorphic. *Proc Natl Acad Sci U S A*. 2008;105:15605–15610.
 64. Van Den Bent MJ, Afra D, De Witte O, et al. Long-term efficacy of early versus delayed radiotherapy for low-grade astrocytoma and oligodendroglioma in adults: The EORTC 22845 randomised trial. *Lancet (London, England)*. 2005;366:985–990.
 65. Chaichana KL, McGirt MJ, Latta J, Olivi A, Quiñones-Hinojosa A. Recurrence and malignant degeneration after resection of adult hemispheric low-grade gliomas. *J Neurosurg*. 2010;112:10–17.
 66. Qiu A, Zhang H, Kennedy BK, Lee A. Spatio-temporal correlates of gene expression and cortical morphology across lifespan and aging. *Neuroimage*. 2021;224:117426.
 67. Váša F, Romero-Garcia R, Kitzbichler MG, et al. Conservative and disruptive modes of adolescent change in human brain functional connectivity. *Proc Natl Acad Sci U S A*. 2020;117:3248–3253.